EMPIRICAL TIDAL DISSIPATION IN EXOPLANET HOSTS FROM TIDAL SPIN–UP

Kaloyan Penev,[1] L. G. Bouma,[2] Joshua N. Winn,[2] and Joel D. Hartman[2]

[1] *Department of Physics, The University of Texas at Dallas, 800 West Campbell Road, Richardson, TX 75080-3021 USA*
[2] *Department of Astrophysical Sciences, Princeton University, 4 Ivy Ln., Princeton, NJ 08544, USA*

ABSTRACT

Stars with hot Jupiters tend to be rotating faster than other stars of the same age and mass. This trend has been attributed to tidal interactions between the star and planet. A constraint on the dissipation parameter $Q'_\star$ follows from the assumption that tides have managed to spin up the star to the observed rate within the age of the system. This technique was applied previously to HATS-18 and WASP-19. Here we analyze the sample of all 188 known hot Jupiters with an orbital period <3.5 days and a "cool" host star ($T_{\rm eff} < 6100\,{\rm K}$). We find evidence that the tidal dissipation parameter ($Q'_\star$) increases sharply with forcing frequency, from 10^5 at 0.5 day^{-1} to 10^7 at 2 day^{-1}. This helps to resolve a number of apparent discrepancies between studies of tidal dissipation in binary stars, hot Jupiters, and warm Jupiters. It may also allow for a hot Jupiter to damp the obliquity of its host star prior to being destroyed by tidal decay.

Keywords: planet-star interactions — stars: rotation — planetary systems

Corresponding author: Kaloyan Penev
kaloyan.penev@utdallas.edu

1. INTRODUCTION

Tidal forces allow astronomical bodies to exchange energy and angular momentum. The friction associated with tidally-induced fluid flow leads to long-term energy dissipation, with profound consequences throughout all of astrophysics. Even when restricting our attention to low-mass stars, there are numerous situations in which tidal dissipation plays a pivotal role:

- A classic question in exoplanetary science is how hot Jupiters (HJs) attain their tight orbits. One proposed answer is that wide-orbiting giant planets can be thrown into high-eccentricity orbits with small periastron distances, which are then shrunk and circularized by tidal dissipation in the planet and the star (Rasio & Ford 1996). Another mechanism for HJ placement invokes interactions with the protoplanetary disk, causing the planet's orbit to spiral inward (Lin et al. 1996). In this scenario the planet arrives very early, when the star is still young and large, and tidal dissipation threatens to cause the planet to spiral further inward and become engulfed. Nelson et al. (2017) recently argued that the observed distribution of orbital distances suggests that both mechanisms might operate.

- Tidally-induced orbital decay has been implicated in the apparent lack of short-period giant planets in globular clusters (Debes & Jackson 2010) and around sub-giant stars (Schlaufman & Winn 2013). There have also been reports of direct detection of period shrinkage for hot Jupiters (*e.g.*, Maciejewski et al. 2016; Patra et al. 2017), although none have been confirmed beyond doubt.

- Many HJs have been found to have orbits that are misaligned with the host star's equatorial plane. The patterns observed within the collection of stellar-obliquity measurements have led to the hypothesis that tidal dissipation has re-aligned many systems that were formerly misaligned (c.f. Winn et al. 2010; Valsecchi & Rasio 2014).

- The mechanisms responsible for tidal dissipation must also operate on stellar pulsations and oscillations. In particular, Gonczi (1981) showed that the red limit of the Cepheid instability strip is very sensitive to the dissipation efficiency, and Goldreich & Kumar (1988) and Goldreich et al. (1994) presented a theory for the amplitudes of solar p-modes in which the results are very sensitive to the dissipation model.

Clearly, a better understanding of the dissipative processes in stars would have broad implications. The endpoint of tidal evolution can often be predicted based on simple considerations of energy and angular momentum, but the rate of evolution cannot yet be predicted from first principles, owing to the complexity and uncertainty in the processes that convert large-scale motions into heat. The rate is traditionally parameterized by the dimensionless quality factor $Q'_\star \equiv Q_\star/k_2$ (Goldreich & Soter 1966), where $Q_\star$ is the inverse of the phase lag between the tidal potential and the tidal bulge, and k_2 is the tidal Love number. There are many theoretical models for tidal dissipation in circulation, giving contradictory predictions for this parameter (cf. Zahn 1975, 1989; Goldreich & Keeley 1977; Goodman & Dickson 1998; Ogilvie & Lin 2004; Penev et al. 2009; Essick & Weinberg 2016).

This work is concerned with tidal interactions between hot Jupiters and their host stars. The very shortest-period giant planets ($P \lesssim$ few days) usually have circular orbits, as expected theoretically due to tidal dissipation within the planet. This represents a state of minimum orbital energy at fixed angular momentum. After reaching this stage, further changes to the orbit must involve the transfer of orbital angular momentum to the rotation of either the star or the planet. Because the planet's rotational angular momentum is many orders of magnitude smaller than that of the orbit, dissipation within the planet cannot possibly cause significant orbital evolution after the orbit is circularized. Stars, on the other hand, have much larger masses and sizes and can exchange large amounts of angular momentum with the orbit. Thus, for the large number of HJs with circular orbits, only the tidal dissipation within the star is important. Dissipation within the star leads to changes in the stellar spin and the orbital period. For the common case in which the stellar rotation period is longer than the orbital period, tides cause the star to spin faster and the orbit to shrink.

Pont (2009) and Husnoo et al. (2012) presented evidence that the stars hosting some of the shortest-period planets have indeed been tidally spun up. Since those studies, many more systems showing excess stellar rotation have been found. Penev et al. (2016) (P16) examined two systems with unusually short periods. Under the assumption that tides have spun up the stars within their estimated ages, they found the allowed range for $\log Q'_\star$ to be 7.2–7.4 for HATS-18 (P16), and 6.5–6.9 for WASP-19 (Hebb et al. 2010). These and most other previous studies have assumed that the $Q'_\star$ parameter is independent of the frequency of the tidal forcing over the range of interest, even though there is no physical

reason to expect this to be the case. Indeed there are strong theoretical reasons to expect $Q'_\star$ to be a sensitive function of frequency (see, e.g., Goldreich 1963; Ogilvie 2014).

In this study, we improve on the sophistication of the P16 analysis, and apply it to 75 systems rather than two. Section 2 describes our method for modeling the combined orbital and stellar spin evolution and deriving constraints on $Q'_\star$. Section 3 presents the results. Section 4 places the results within the context of other available constraints on $Q'_\star$, and discusses the implications for HJ systems, including the possibility of tidal realignment of the stellar obliquity in HJ systems.

2. METHODS

2.1. *Orbital and Stellar Spin Evolution*

We model each hot Jupiter system using the Planetary Orbital Evolution due to Tides (POET) code (Penev et al. 2014). POET has had numerous upgrades since its initial release. The version used in this work self-consistently tracks the orbital decay, the accompanying evolution of the stellar spin period and obliquity, the loss of angular momentum due to the stellar wind, and the changes in the star's radius and moment of inertia over the course of stellar evolution. The tidal dissipation rate is allowed to be an arbitrary prescribed function of the system properties. For the time being, POET is restricted to circular orbits and does not allow for any thermal evolution of the planet. For simplicity, we assumed zero obliquity throughout most of this study. Some preliminary investigations of obliquity evolution are described in § 4.

Orbital evolution—The orbital evolution equations are those specified by Lai (2012). These equations are general enough to accommodate any prescribed frequency-dependence of the tidal dissipation rate, and POET also has this flexibility.

Stellar spin evolution—Our model for stellar spin-down is similar to that used by Irwin et al. (2007), and was described in detail by P16. In brief, the star is divided into a radiative core and a convective envelope which can have different rotation periods. The convective zone loses angular momentum due to a magnetized wind. Friction acts to gradually torque the two zones toward synchronous rotation. We adopt the coupling timescale for core-envelope angular momentum exchange from the models of Gallet & Bouvier (2015), and wind strength parameters from Irwin et al. (2007). Recently van Saders et al. (2016) presented evidence for a possible loss of spin-down efficiency at long spin periods; while interesting, this does not affect the results of our
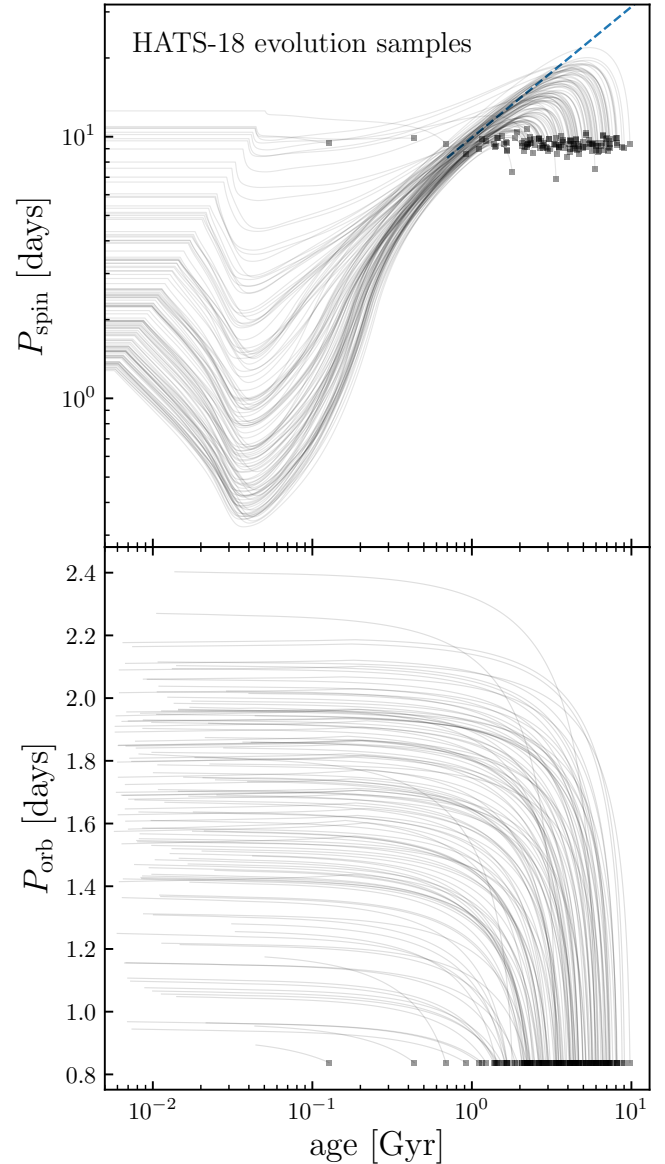

Figure 1. *Top.*—Possible histories of the spin period of the HATS-18 system, based on our model for tidal evolution. Each curve shows the calculated evolution for a set of system parameters drawn randomly from distributions representing the observational uncertainties. The squares are random samples of the current spin period and system age. The dashed line is the Skumanich relation ($P_{\rm spin} \propto t^{1/2}$) which would apply in the absence of a planet. *Bottom.*— Same, for the orbital period. To determine constraints on $Q'_\star$ we marginalize over the uncertainties in all the observed parameters.

study, since none of the systems that give meaningful constraints on $Q'_\star$ have stars that spin so slowly.

Stellar evolution—The orbital and stellar spin evolution depend on the stellar radius and mass, the moments

of inertia of the radiative and convective zones, and on the location of the core-envelope boundary. To track the evolution of these quantities over time, we generate a grid of isochrones using Modules for Experiments in Stellar Astrophysics (MESA; Paxton et al. 2011, 2013, 2015). We use the solar-tuned inlists from the MESA Isochrones and Stellar Tracks (MIST) project (Choi et al. 2016; Dotter 2016). The MIST isochrones have been validated over a wide range of masses, metallicities, and phases of stellar evolution, by comparison to existing databases. We downloaded the relevant input files and, with minor modifications, computed grids of stellar evolutionary models spanning all the relevant parameters of our sample.[1] It was not possible to simply use the published model outputs, since they did not include the evolution of the convective and radiative moments of inertia or of the location of the boundary between the two zones. To compute the two moments of inertia and the location of the boundary, we identified the tachocline using the mixing types of each radial cell, and then performed the moment-of-inertia integral using the density profile $\rho(r)$ at each time step. We then interpolated over stellar metallicity and mass to find the stellar properties corresponding to a given planet-star system at any time in its evolution (see Penev et al. 2014, Appendix C).

Sub and super-synchronous rotation—All the stars in our sample have spin periods that are longer than the planet's orbital period, but in our calculations we do not assume that this was always the case. For some systems in our sample, the early evolution goes through a brief period during which the star spins super-synchronously, and thus the direction of orbital and stellar spin evolution is reversed. In practice this does not have a significant effect on the results, because the time intervals of super-synchronous rotation are brief, and more generally because of the lack of sensitivity of the current-day parameters to the initial spin period (as explained below).

Spin-orbit locking—POET follows all of the relevant physics of sub- and super-synchronous tidal coupling and the changes in the star's moment of inertia over the course of stellar evolution, including the possibility that the star-planet system is temporarily locked in

spin-orbit synchrony. Indeed, in the tidal evolution calculations to be described below, we observed some cases in which the planets are able to achieve spin-orbit synchrony with their stars. But the synchrony is almost always temporary. As the star continues to lose angular momentum through its wind, its tidal bulge begins to lag behind the planet, torquing the planet into a lower and faster orbit. To maintain synchrony the star must therefore be spun up even faster. This further increases the rate of angular momentum loss due to the wind. Thus there ensues a positive feedback spiral. Ultimately there comes a time at which the rate of tidal dissipation is insufficient to maintain synchrony, and the spin-orbit lock is lost. This same process operates in binary star systems. However, due to the much larger secondary mass, the timescale for breaking spin-orbit synchrony is three orders of magnitude longer, typically exceeding the age of the universe. More details were given by Penev et al. (2014) who presented an earlier version of the code.

2.2. *Method of Constraining $Q'_\star$*

We selected all the known transiting planets from the NASA exoplanet archive[2] for which the planet mass exceeds $0.1\,M_{\rm Jup}$, the orbital period is shorter than $3.5\,{\rm days}$, and the star has an effective temperature below $6100\,{\rm K}$. The effective temperature cut-off ensures that only stars with surface convective zones are included in the analysis. We decided to focus on these "cool" stars because both theoretical expectations and observations suggest the dominant tidal dissipation mechanism, and hence its efficiency, is dramatically different for stars without a significant surface convective zone. The restrictions on planet mass and orbital period were designed to select systems with strong tides, for which the host stars are most likely to have been measurably spun up. This resulted in an initial sample of 188 systems.

To model the coupled orbital and spin evolution of each system, we assume that $Q'_\star$ is constant in time, within a given system. However, each system is allowed to have an independent value of $Q'_\star$. For each system we asked which value of $Q'_\star$ leads to enough spin-up to explain the observed rotation rate at the present age, starting from an initial condition compatible with observations of single stars of the same mass within young clusters. Some of the key parameters, such as age and spin period, are subject to large uncertainties. An important part of the work was marginalizing over those uncertainties. We use a Monte Carlo technique. The likelihood is computed as follows:

---

[1] Input files retrieved 2016-09-20 from http://waps.cfa.harvard.edu/MIST/data/tarballs_v1.0/MESA_files.tar.gz. As a check on the models, we were able to reproduce the results of Choi et al. (2016). Our minor modifications were to use the fine-tuned protosolar abundances discussed in Sec. 4 of Choi et al. (2016), rather than the published grids. We opted for those abundances for greater consistency with the helioseismic models of the Sun (Christensen-Dalsgaard et al. 1996).

[2] exoplanetarchive.ipac.caltech.edu/

1. Draw random samples for the radial-velocity semi-amplitude, transit characteristics (period, depth, and duration), stellar effective temperature, metallicity, and spin period from distributions based on the observational uncertainties. For each parameter we adopt a Gaussian probability distribution centered on the value quoted in the literature, with a standard deviation given by the quoted 1σ uncertainty.

2. From these samples, compute the posterior distributions for the stellar and planetary mass, and the system age (based on the MESA models).

3. Draw a random value for $\log_{10} Q'_\star$ from a uniform distribution between 4–9.

4. Draw a random value for the initial stellar spin period, based on the measured spins of stars of similar mass from the Pleiades and M 50 clusters (which have an approximate age of 133 Myrs).

5. Determine the initial orbital period for which the evolution computed by POET brings the system to the currently observed orbital period at the system age chosen in step 2.

6. Compute the likelihood by comparing the observed stellar spin period to the calculated spin period at the current age that is predicted by the orbital evolution model. Stellar spin periods are taken from photometric measurements whenever available, and otherwise from $v \sin i$ measurements. The uncertainty distribution for the stellar spin is assumed to be Gaussian, with an appropriate mean and standard deviation.

Thus, for each system, the posterior probability distribution is constructed for $\log_{10}(Q'_\star)$, accounting for all the observational uncertainties. As noted above, we assume the orbit to be circular, we neglect obliquity evolution, and we also neglect the uncertainties in the spindown model parameters. Fig. 1 shows some examples of the calculated time evolution of the stellar spin and planetary orbital period for the HATS-18 system. In the top panel, the dashed line shows the Skumanich relation ($P_{\rm spin} \propto t^{1/2}$) which would apply in the absence of a planet. The observed present-day spin period (represented by the squares in Fig. 1) is lower than one would expect without the tidal torque from a hot Jupiter.

The top panel of Fig. 1 shows that the broad initial distribution of stellar spin periods collapses to a much narrower range after ≈ 500 Myr of evolution. This generic feature of stellar spin-down is caused by the angular momentum loss due to the magnetized stellar wind (Schatzman 1962; Weber & Davis 1967; Skumanich 1972): more rapidly rotating stars experience stronger magnetic braking. At least initially, the presence of a HJ does not affect this well-known feature of stellar spin evolution. In other words, the relation between stellar mass, spin period, and age that is observed in open clusters is preserved for a few hundred Myrs after the zero-age main sequence. However, once the host star starts spinning slowly enough (in Fig. 1, at $P_{\rm spin} \approx 15$ days, age $\approx 1 - 2$ Gyr), the rate of angular momentum loss through the magnetized wind is matched by the rate of angular momentum gain from tidal interactions with the planet. At this time, the star begins spinning up, and it continues to gain angular momentum until it reaches its present-day spin period.

The stellar spin at an age of ≈ 500 Myr hardly depends at all on the spin at earlier times (Fig. 1). This implies that the choice of which young clusters to use as references for the initial rotation period is relatively unimportant. Because the early history of the stellar spin is quickly forgotten, the inferred value of $Q'_\star$ can be loosely interpreted as a measure of the present-day value of $Q'_\star$, i.e., even if in reality $Q'_\star$ has changed over time, in contradiction with the premise of our evolution calculations, we will infer a value of $Q'_\star$ representative of the present-day value (as shown quantitatively in § 3.1).

For the same reason, our results for $Q'_\star$ do not depend on the unknown events that lead to the formation of the HJs, provided they take place within the first few hundred million years of the system. Whether hot Jupiters arrive in their tight orbits within the first million years through disk migration, or 200 Myr later through some other process such as high-eccentricity migration, the final stellar spin is hardly affected. We note, though, that the proposed high-eccentricity mechanisms for hot Jupiter formation (see, e.g. Fabrycky & Tremaine 2007) operate on a very wide range of timescales, up to billions of years. If the long-timescale mechanisms were dominant then the actual time for tidal evolution would be shorter than is assumed in our calculations. This caveat should be kept in mind, although many studies have concluded that the high-eccentricity mechanism is unlikely to be the dominant mechanism for producing HJs (see, e.g. Naoz et al. 2012; Crida & Batygin 2014; Dawson et al. 2015; Petrovich 2015; Ngo et al. 2015, 2016; Schlaufman & Winn 2016).

3. RESULTS

Of the 188 systems in the sample, our procedure led to two-sided limits on $Q'_\star$ for 35 systems. In another 40 cases, it was possible to derive a lower bound on $Q'_\star$. In the remaining cases the data did not lead to mean-
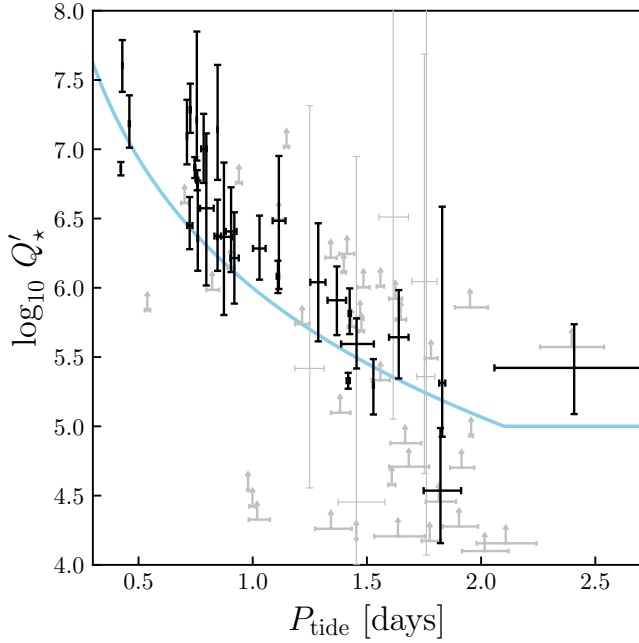
Figure 2. Evidence for the frequency-dependence of $Q'_\star$. Shown are the values of $Q'_\star$ inferred for each system, as a function of the tidal forcing period. Black points are cases for which $Q'_\star$ was bounded to within two orders of magnitude. Thinner gray symbols are cases for which the two-sided limits span more than two orders of magnitude. Gray arrows indicate lower limits. The blue curve is a saturated power-law fit to the points with two-sided limits (Eq. 2).

Figure 3. Tentative evidence for a secondary dependence of $Q'_\star$ on the stellar spin rate. Shown are the values of $Q'_\star$ inferred for selected systems, as a function of a dimensionless spin parameter. The blue symbols correspond to systems with tidal periods from 0.7 to 0.9 days, and the orange symbols are for tidal periods from 1.3 to 1.5 days. The blue curve (a power-law dependence) is a fit to blue symbols with two-sided limits. For the orange line, only the offset was fitted, while the slope was forced to be the same as the blue line.

ingful constraints. Table 1 summarizes the quantitative results for each system. Fig. 2 shows the inferred value of $\log_{10}(Q'_\star)$ for each system, as a function of the tidal forcing period. The tidal forcing period is one-half of the orbital period of the planet in a reference frame rotating with the stellar spin:

$$P_{\rm tide} \equiv \frac{1}{2(P_{\rm orb}^{-1} - P_{\rm spin}^{-1})}. \qquad (1)$$

We see a clear trend toward larger $Q'_\star$ with decreasing $P_{\rm tide}$. The blue line is a simple function that fits the period dependence,

$$Q'_\star(P_{\rm tide}) = \max\left[\frac{10^{6.0}}{(P_{\rm tide}/{\rm days})^{3.1}}, 10^5\right]. \qquad (2)$$

The minimum value of $Q'_\star = 10^5$ was imposed because it agrees with the constraints obtained by Milliman et al. (2014) (M14, hereafter) based on observations of the eccentricity-period relation for binary stars in open clusters. This minimum value is also consistent with the results from the longest-period systems in our sample.

About half of the systems for which two-sided constraints were obtained have tidal periods in the relatively
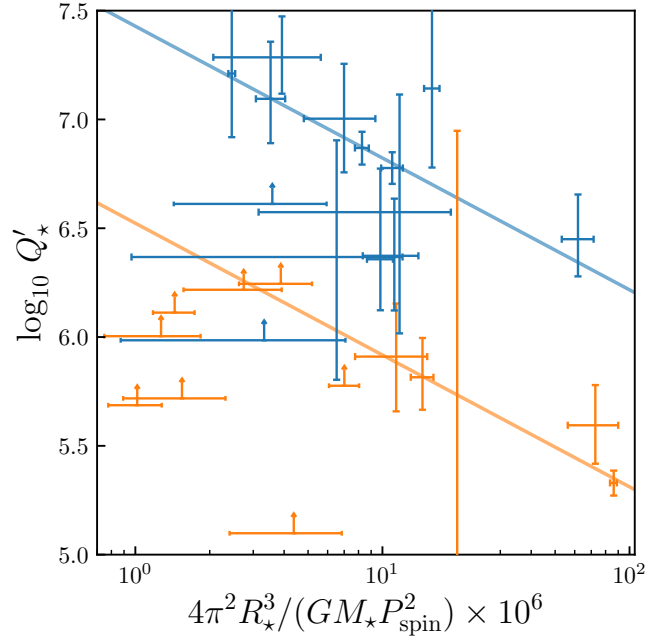
narrow range $P_{\rm tide}$ = 0.7–0.9 day. This allows us to check for any secondary dependence of $Q'_\star$ on other system parameters, at fixed period. We looked for trends with the planet mass, stellar mass, and stellar spin. Of these, the spin showed the strongest correlation with $Q'_\star$, with a formal false alarm probability of 5.5×10^{-4}. Fig. 3 displays this result as a correlation between $Q'_\star$ and the dimensionless parameter

$$\left(\frac{\Omega_{\rm spin}}{\Omega_{\rm crit}}\right)^2 = \left[\frac{(2\pi/P_{\rm spin})}{\sqrt{GM_\star/R_\star^3}}\right]^2 = \frac{4\pi^2 R_\star^3}{GM_\star P_{\rm spin}^2}, \qquad (3)$$

where $\Omega_{\rm crit}$ is the critical angular velocity for breakup due to centrifugal forces. In this figure the blue points are the systems with $P_{\rm tide}$ = 0.7–0.9 d. The orange points are a separate set of systems with $P_{\rm tide}$ in the range from 1.3-1.5 days. By itself, the orange collection of points would not be sufficient to establish that a correlation exists, but they are at least consistent with the same slope that fits the blue points.
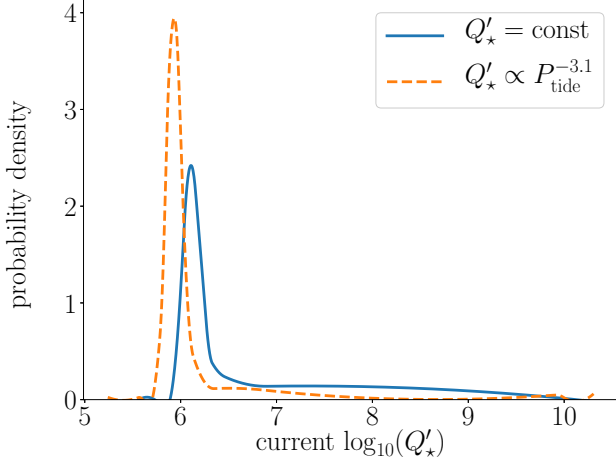
3.1. Self-consistency of results

Figure 4. Probability distributions for the present day $Q'_\star$ for WASP-50, computed under the assumption of a frequency-independent $Q'_\star$ (solid), and the frequency-dependent prescription for $Q'_\star$ found in § 3 (dashed). The constraints are similar, supporting the claim that our results are reliable even though they were derived under the assumption that $Q'_\star$ = constant for each system.

Our calculations assumed that $Q'_\star$ is a constant in time, while the results suggest that it actually depends sharply on frequency. To investigate the systematic error associated with this inconsistency, we repeated the calculations but this time requiring $Q'_\star \propto P_{\text{tide}}^{3.1}$, with a normalization that is specific to each system. However, since it would require additional months of computing time to perform another iteration of the entire calculation, we confirmed that the systematic errors are relatively small through two more tractable calculations.

First we repeated the analysis of the WASP-50 system, which gives the tightest constraint on $Q'_\star$ near the middle of the period range of our sample. We found that the inferred value of $Q'_\star$ differs by 0.2 dex from the case in which we assumed $Q'_\star$ to be a constant, as shown in Fig. 4. Similar tests, with similar results, had already been performed by Penev et al. (2016) for the two shortest-period systems in the sample, HATS-18 and WASP-19.

Next we repeated the analysis for all the most important members of the sample, but without the computationally expensive marginalization over all of the observational uncertainties. We analyzed all the systems that gave two-sided limits in Sec. 2.2. For each system we took the initial spin period to be the median of the measured periods in the Pleiades/M 50 samples, and adopted stellar and planetary parameters based on the best-fit values reported in the literature. Then, under
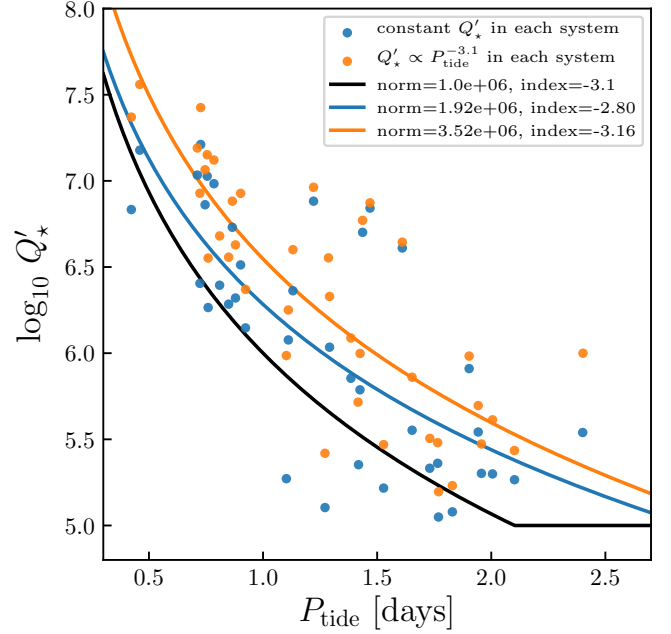

Figure 5. Estimate of how the assumed $Q'_\star(P_{\text{tide}})$ dependence affects the derived $Q'_\star(P_{\text{tide}})$ relation. The displayed points come from the method described in Sec. 3.1. The blue points assume $Q'_\star(P_{\text{tide}})$ = constant, and the fit (blue line) weights these points uniformly. The orange points assume $Q'_\star(P_{\text{tide}}) = Q_0 P_{\text{tide}}^{-3.1}$, and solves for an appropriate Q_0 (see text). The orange line weights orange points equally. The black line (Eq. 2) is the same as from Fig. 2, which was found by applying the method described in Sec. 2.2. Regardless of the assumed frequency scaling for each system, and regardless of the assigned weights each system receives, stars that are forced faster dissipate less efficiently.

the assumption

$$Q'_\star = \max \left[Q_0 \times \left(\frac{P_{\text{tide}}}{\text{days}} \right)^{-3.1}, \ 10^5 \right], \qquad (4)$$

we determined the values Q_0 and the initial orbital period that lead to a good match between the calculated and observed values of the present-day orbital and spin periods (or $v \sin i$, when the period is not available).

The orange points in Fig. 5 show the results of this exercise. An unweighted power-law fit to the collection of results gives $Q'_\star \propto P_{\text{tide}}^{-3.1}$. The blue points show the results of performing exactly the same procedure under the assumption $Q'_\star$ = constant for each system; here the power-law fit gives $Q'_\star \propto P_{\text{tide}}^{-2.8}$. The overall normalizations differ by about a factor of two. We consider this to be good agreement, and a sign that no further steps toward total self-consistency are warranted. The results also show that the results reported in Fig. 2 and Table 1 are subject to systematic uncertainties of about

a factor of two, in addition to the reported statistical uncertainties.

We had anticipated that the inferred present-day $Q'_\star$ values would be insensitive to the system's history because of the strong dependence of magnetic braking on the stellar spin frequency. The faster the spin, the faster angular momentum is lost. In the absence of tides, this relationship is what causes the spin rates of initially fast and slow rotators to converge over time, leading to the well known "gyrochronological" relationship between age and rotation rate. In the case of tidal spin-up, spinning up the star at early times has hardly any effect on the present-day properties because the excess angular momentum is quickly lost due to the enhanced magnetic braking. As a result, any excess spin that can be detected now is a measure of only the most recent history of angular momentum deposition.

4. DISCUSSION

4.1. Other Empirical Constraints on $Q'_\star$

Meibom & Mathieu (2005) (hereafter, MM05) and Milliman et al. (2014) (M14) examined the eccentricity distribution of binaries within open clusters of differing ages. For each cluster they tried to find the orbital period P_{circ} below which binaries have been tidally circularized and above which they have not yet circularized. They determined $Q'_\star$ by fitting the trend of P_{circ} with age, thereby assuming $Q'_\star$ to be the same for all stars, ages, and tidal periods. These authors argued that significant circularization occurs on the main-sequence, requiring $Q'_\star \lesssim 10^{5.5}$. However there are some puzzling results that call into question the premises of this method. The observed P_{circ} is not a monotonic function of age: Praesepe and the Hyades (630 Myr) have smaller values of P_{circ} than the younger clusters. Also notable is that NGC 6819 (2.5 Gyr) is a large outlier from the overall main-sequence circularization trend. Thus, three out of the seven clusters used in that study are inconsistent with the claimed result. In any case, the existence of a particular P_{circ} must be an oversimplification because all the clusters show a significant overlap in orbital period between circularized and highly eccentric systems (cf. Mazeh 2008). Furthermore, taking the conclusions of MM05 and M14 at face value, one would predict unrealistically rapid rates for the orbital decay of HJs. To avoid destroying too many HJs, Penev et al. (2012) (P12) argued that $Q'_\star$ must exceed 10^7.

Tidal dissipation also appears to have shaped the eccentricity distribution of short-period giant planets. By integrating the tidal evolution equations backward in time for the shortest-period hot Jupiters, and requiring their initial eccentricity distribution to match that of warm Jupiters (longer-period planets of similar mass), Jackson et al. (2008) found $Q'_p \sim 10^{5.5}$ for the planets, and $Q'_\star \sim 10^{6.5}$ (with a large uncertainty) for the stars. Similar results were obtained by Husnoo et al. (2012). On the other hand, Hansen (2010) interpreted the same data using a different formalism, in which the tidal dissipation rate was allowed to vary as expected with the size of the body and its orbital distance. He found lower dissipation rates of $10^7 < Q'_p < 10^8$ and $10^7 < Q'_\star < 10^9$. Most recently Bonomo et al. (2017), using the most up-to-date observations of transiting HJs and simple timescale arguments, found that $Q'_\star$ has to exceed 10^6 or 10^7 (depending on the system) and $10^5 < Q'_p < 10^9$.

Our results suggest a possible reconciliation of all of these confusing and seemingly inconsistent results. At the shortest-period end, we find $Q'_\star \sim 10^7$ which is consistent with the previous study of tidal inspiral by Penev et al. (2012). For the longest periods in our sample we found $Q'_\star \sim 10^5$, which is compatible with the trend of circularization period versus age in cluster binaries seen by Meibom & Mathieu (2005) and Milliman et al. (2014), and with most of the constraints based on hot and warm Jupiters (Jackson et al. 2008; Husnoo et al. 2012). This leaves only the higher $Q'_\star$ values found by Hansen (2010). Regarding those, we note that the results hinge on the observed non-circular orbits of WASP-14b, XO-3b and HAT-P-2b. Those particular planet-hosting stars are right on the boundary between being convective or radiative near the surface. They may have radiative envelopes, or at least exist in a different, much less efficient, regime of tidal dissipation due to the extremely thin convective zone.

4.2. Tidal Alignment of Hot Jupiter Systems

Observations have revealed a wide range of obliquities for the host stars of HJs, including very well-aligned systems (e.g. Winn et al. 2006), strongly misaligned systems (Hébrard et al. 2008), and even polar and retrograde orbits (Winn et al. 2009; Narita et al. 2009; Queloz et al. 2010). The basis for most of these results is the Rossiter-McLaughlin effect, a spectroscopic distortion that occurs during transits. A pattern has emerged from these results: the host stars cool enough to have outer convective zones tend to have low obliquities, while hotter stars show a broader range of obliquities (Winn et al. 2010; Albrecht et al. 2012).

One possible interpretation is that HJs generally form with a broad range of orbital orientations, and that only the cool stars are able to tidally re-align the system due to the enhanced tidal dissipation rate associated with outer convective zones. A problem with this interpretation is that simple tidal models predict that stellar re-
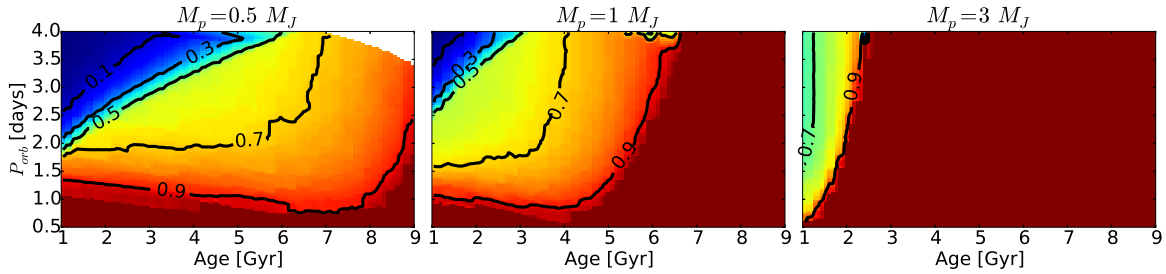
Figure 6. Fraction of initial spin–orbit orientations that end up aligned by a given age and with a given orbital period due to orbital evolution, assuming the frequency-dependent $Q'_\star$ given by Eqn. 2. The host star is 1 $M_\odot$ in all cases. The spin-down parameters are taken from (Irwin et al. 2007), and the three panels are for planet masses of 0.5, 1 and 3 $M_{\rm Jup}$.

alignment should occur on the same timescale as orbital decay, making it unlikely that we would ever observe a re-aligned hot Jupiter system. Whether or not there are viable mechanisms for re-alignment that are faster than orbital decay is an outstanding theoretical question (Lai 2012; Rogers & Lin 2013; Li & Winn 2016).

Our finding of a strongly frequency-dependent $Q'_\star$ is relevant to this issue. As elucidated by Lai (2012), the timescales for obliquity damping and orbital decay can be different, provided that a system is misaligned. In particular, the obliquity can be affected by tidal waves with much lower frequency ($2\Omega_{\rm spin}$) than the ones causing tidal decay ($\sim 2\Omega_{\rm orb}$). The frequency dependence of $Q'_\star$ suggested by our study may allow a way for the stellar obliquity to be damped to a low value, before the orbit decays. This increases the chance of discovering a low obliquity system before the planet is destroyed. Fig. 6 shows the results of our preliminary investigation of this issue, using nominal system parameters rather than the actual parameters of the known systems. We considered a solar-mass star, a planet with one of three possible masses, and an initial obliquity chosen from an isotropic distribution. The contours in this figure show the fraction of planet–star systems for which the obliquity damps to below 5° before the planet is tidally destroyed, as a function of the age and observed orbital period. The evolution was calculated using the prescription for $Q'_\star$ given by Eq. 2.

The results — obtained without tuning any free parameters — show that obliquity damping is achieved over much of the relevant parameter space. This is an enticing result: it suggests that the frequency-dependence of tidal dissipation which we have inferred from stellar spin-up could be sufficient to explain the high degree of alignment observed for planets around stars with surface convective zones without driving the planet into the star through orbital decay. We intend to investigate this issue more rigorously in the future, with a detailed system-by-system evaluation and a comparison with the measured obliquity distribution. If successful, then we might be able to explain the observed obliquity pattern while also providing information about the initial distribution of stellar obliquities.

4.3. Conclusions & Caveats

By modeling the tidal evolution of a large sample of hot Jupiters orbiting main-sequence stars with external convection zones, we have derived limits on the dissipation parameter $Q'_\star$ and found evidence for a strong frequency dependence of this parameter (Fig. 2), while systems with similar tidal forcing periods led to similar results for $Q'_\star$. There is also a possible correlation between $Q'_\star$ and the stellar spin frequency, at constant tidal period (Fig. 3). At the shortest tidal periods, $Q'_\star$ matches the Penev et al. (2012) constraints from exoplanet inspiral, while at the longest periods $Q'_\star$ matches the Milliman et al. (2014) constraints from open cluster binary star circularization, thus reconciling those seemingly inconsistent results. We also showed that with no further free parameters, our prescription for the frequency-dependent $Q'_\star$ might naturally explain the fact that HJs around cool stars tend to be in nearly perfectly equatorial orbits around their stars, while those around hotter stars have a broader range of orbital orientations.

We can think of many ways to improve on our analysis, mainly for self-consistency. It might be warranted to attempt a hierarchical Bayesian analysis, in which the constant-$Q'_\star$ model is replaced with

$$Q'_\star = Q'_0 \left(\frac{P_{\rm tide}}{\rm day}\right)^\alpha \left(\frac{\Omega_{\rm spin}}{\Omega_{\rm crit}}\right)^\beta, \qquad (5)$$

where $P_{\rm tide}$ is defined by Eq. 1, and the parameters Q'_0, α and β are determined by modeling all of the systems simultaneously. As in Section 3, the purpose of the second factor is to allow for an explicit dependence on stellar spin rate, even for a fixed tidal forcing period. Such a dependence could arise from rotationally induced changes in the structure of the star and the oscillations it supports. Our initial explorations (Sec. 3.1) suggest that moving toward this level of self-consistency could affect

the inferred normalization Q'_0 by about a factor of two, and the exponent by about 0.2. We also found tentative evidence for a nonzero value of β. In principle, if β turns out to be too large, the spin-dependence of the tidal dissipation rate could overwhelm the spin-dependence of magnetic braking. This would lead to a more sensitive (and problematic) dependence of our results on the initial conditions. The current data, though, give no suggestion that β is large enough for this situation to occur.

Another consideration is that if the tidal dissipation in cool stars is responsible for the spin-orbit alignment of HJ systems, then self-consistency requires a consideration of the initial obliquity distribution of the stars. Based on the numerical experiments of P16 (see their Fig. 10), allowing for a wide range of initial obliquities has the effect of extending the allowed range of $Q'_\star$ to lower values.

Another limitation of our study is that we neglected the uncertainties in the parameters of the spin-down model. For instance, based on Fig. 8 of Gallet & Bouvier (2015), we assumed a constant core-envelope coupling timescale of 10 Myr. While these authors found that to be appropriate for stars with masses comparable to the Sun, they also found evidence that this parameter should really be a function of the amount of differential rotation, with faster coupling for strong differential rotation. We adopted the value corresponding to large differential rotation because that is the regime where this parameter has the strongest effect. However, a more complete treatment would marginalize over the possible values for this timescale, as well as the parameters in the model of magnetic braking. Again we do not expect the results would change dramatically, since for the two systems considered by P16 the results were robust even to implausibly large changes in the coupling timescale and spin-down parameters.

Another detail is that the stellar-evolutionary models we relied upon do not include any effects of stellar rotation. Although stellar rotation has only a minor impact on the bulk stellar properties for low-mass stars, this may be worth including for self-consistency in future studies.

APPENDIX

Table 1. Derived stellar quality factors for all systems with single or two-sided constraints.

System	Orbital Period [days]	Spin Period [days]	Stellar Mass [$M_\odot$]	Stellar Radius [$R_\odot$]	Planetary Mass [M_J]	Planetary Radius [R_J]	$\log_{10}(Q'_\star)$
CoRoT-12	$2.83 \pm 1.3 \times 10^{-5}$	$6 \times 10^1 \pm 6 \times 10^1$	$1.08^{+0.08}_{-0.07}$	$1.12^{+0.1}_{-0.09}$	$0.917^{+0.07}_{-0.065}$	1.44 ± 0.13	>5.33
CoRoT-18	$1.9 \pm 2.8 \times 10^{-6}$	5.4 ± 0.5	0.95 ± 0.15	1 ± 0.13	3.5 ± 0.38	1.3 ± 0.18	$5.59^{+0.185}_{-0.177}$
CoRoT-2	$1.74 \pm 1 \times 10^{-6}$	4.5 ± 0.5	0.96 ± 0.08	0.91 ± 0.03	3.47 ± 0.22	$1.47^{+0.042}_{-0.044}$	$5.33^{+0.0565}_{-0.0582}$
CoRoT-29	$2.85 \pm 6 \times 10^{-6}$	13 ± 2.5	0.97 ± 0.14	0.9 ± 0.12	0.85 ± 0.2	0.9 ± 0.16	$4.54^{+0.452}_{-0.379}$
HAT-P-13	$2.92 \pm 1.5 \times 10^{-5}$	48 ± 11	$1.22^{+0.05}_{-0.1}$	1.56 ± 0.08	0.851 ± 0.038	1.28 ± 0.079	>6.01
HAT-P-20	$2.88 \pm 4 \times 10^{-6}$	7.28 ± 0.5	0.76 ± 0.03	0.69 ± 0.02	7.25 ± 0.187	0.867 ± 0.033	>5.57
HAT-P-23	$1.21 \pm 1.7 \times 10^{-7}$	6.81 ± 0.46	1.1 ± 0.05	1.09 ± 0.03	2.07 ± 0.12	1.37 ± 0.09	$6.45^{+0.205}_{-0.171}$
HAT-P-27	$3.04^{+5 \times 10^{-6}}_{-6 \times 10^{-6}}$	$1 \times 10^2 \pm 1 \times 10^2$	0.94 ± 0.04	$0.9^{+0.05}_{-0.04}$	0.62 ± 0.03	$1.04^{+0.077}_{-0.058}$	>5.77
HAT-P-28	$3.26 \pm 7 \times 10^{-6}$	$3 \times 10^2 \pm 5 \times 10^2$	1.02 ± 0.05	$1.1^{+0.09}_{-0.07}$	0.626 ± 0.037	$1.19^{+0.102}_{-0.075}$	>5.49
HAT-P-36	$1.33 \pm 3 \times 10^{-6}$	15.3 ± 0.5	1.02 ± 0.05	1.1 ± 0.06	1.83 ± 0.099	1.26 ± 0.071	$7.29^{+0.188}_{-0.167}$
HAT-P-37	$2.8 \pm 7 \times 10^{-6}$	15 ± 2.6	0.93 ± 0.04	0.88 ± 0.06	1.17 ± 0.103	1.18 ± 0.077	>4.71
HAT-P-43	$3.33 \pm 1.5 \times 10^{-5}$	23 ± 4.9	$1.05^{+0.03}_{-0.04}$	$1.1^{+0.04}_{-0.02}$	0.662 ± 0.06	$1.28^{+0.057}_{-0.034}$	>4.70
HAT-P-52	$2.75 \pm 9.4 \times 10^{-6}$	75 ± 63	0.89 ± 0.03	0.89 ± 0.05	0.818 ± 0.029	1.01 ± 0.072	>6.00
HAT-P-53	$1.96 \pm 3.9 \times 10^{-6}$	15 ± 2	1.09 ± 0.04	$1.21^{+0.08}_{-0.06}$	1.48 ± 0.056	1.32 ± 0.091	$6.48^{+0.468}_{-0.493}$
HAT-P-65	$2.61 \pm 3.1 \times 10^{-6}$	13.3 ± 1.17	1.21 ± 0.05	1.86 ± 0.1	0.53 ± 0.083	1.89 ± 0.13	$4.5^{+2.5}_{-0.45}$
HATS-14	$2.77 \pm 2.7 \times 10^{-6}$	12 ± 3.9	0.97 ± 0.02	$0.93^{+0.02}_{-0.01}$	1.07 ± 0.07	$1.04^{+0.032}_{-0.022}$	>4.21
HATS-15	$1.75 \pm 9.4 \times 10^{-7}$	11 ± 1.4	0.87 ± 0.02	0.92 ± 0.03	2.17 ± 0.15	1.1 ± 0.04	$6.28^{+0.237}_{-0.225}$
HATS-16	$2.69 \pm 1.1 \times 10^{-5}$	6.1 ± 1	0.97 ± 0.04	$1.24^{+0.1}_{-0.13}$	3.27 ± 0.19	1.3 ± 0.15	$5.42^{+0.315}_{-0.334}$

Table 1 *(continued)*

System	Orbital Period	Spin Period	Stellar Mass	Stellar Radius	Planetary Mass	Planetary Radius	$\log_{10}(Q'_\star)$
	[days]	[days]	[M$_\odot$]	[R$_\odot$]	[M$_J$]	[R$_J$]	
HATS-18	$0.838 \pm 4.7 \times 10^{-7}$	9.4 ± 0.5	1.04 ± 0.047	$1.02^{+0.031}_{-0.057}$	1.98 ± 0.077	$1.34^{+0.049}_{-0.102}$	$7.18^{+0.205}_{-0.173}$
HATS-2	$1.35 \pm 1 \times 10^{-6}$	12.5 ± 0.5	0.88 ± 0.04	0.9 ± 0.02	1.3 ± 0.15	0.776 ± 0.055	$6.36^{+0.417}_{-0.234}$
HATS-23	$2.16 \pm 4.5 \times 10^{-6}$	13 ± 1.6	1.12 ± 0.05	$1.2^{+0.06}_{-0.08}$	1.47 ± 0.072	$1.9^{+0.3}_{-0.4}$	$6.04^{+0.426}_{-0.427}$
HATS-30	$3.17 \pm 2.6 \times 10^{-6}$	13 ± 1.7	1.09 ± 0.03	1.06 ± 0.04	0.706 ± 0.039	1.18 ± 0.052	>4.10
HATS-32	$2.81 \pm 5.5 \times 10^{-6}$	16 ± 3.2	1.1 ± 0.04	$1.1^{+0.1}_{-0.06}$	0.92 ± 0.1	$1.25^{+0.144}_{-0.096}$	>4.88
HATS-33	$2.55 \pm 6.1 \times 10^{-6}$	19 ± 1	1.06 ± 0.03	$1.02^{+0.05}_{-0.04}$	1.19 ± 0.053	$1.23^{+0.112}_{-0.081}$	>5.78
HATS-34	$2.11 \pm 4.7 \times 10^{-6}$	12 ± 1.8	0.95 ± 0.03	0.98 ± 0.05	0.941 ± 0.072	1.4 ± 0.19	$5.4^{+1.9}_{-0.86}$
HATS-4	$2.52 \pm 2 \times 10^{-6}$	67 ± 48	1 ± 0.02	0.93 ± 0.02	1.32 ± 0.028	1.02 ± 0.037	>6.24
HATS-9	$1.92 \pm 5.2 \times 10^{-6}$	17 ± 3.3	1.03 ± 0.039	$1.5^{+0.043}_{-0.101}$	0.837 ± 0.029	1.06 ± 0.098	>4.33
K2-60	$3 \pm 4 \times 10^{-5}$	26 ± 6	0.97 ± 0.07	1.12 ± 0.05	0.426 ± 0.037	0.683 ± 0.037	>4.58
KELT-14	$1.71^{+3.2 \times 10^{-6}}_{-2.6 \times 10^{-6}}$	23 ± 5.7	1.24 ± 0.04	1.52 ± 0.03	1.28 ± 0.032	1.74 ± 0.047	>6.15
KELT-8	3.24 ± 0.00016	23 ± 9.4	$1.21^{+0.08}_{-0.07}$	$1.67^{+0.14}_{-0.12}$	$0.867^{+0.065}_{-0.061}$	$1.86^{+0.18}_{-0.16}$	>4.17
Kepler-17	$1.49 \pm 2 \times 10^{-7}$	12.2 ± 0.029	1.16 ± 0.06	1.05 ± 0.03	2.45 ± 0.11	1.31 ± 0.02	$7.14^{+0.466}_{-0.363}$
Kepler-41	$1.86 \pm 5.2 \times 10^{-7}$	11 ± 3.6	1.15 ± 0.04	1.29 ± 0.02	0.56 ± 0.08	1.29 ± 0.02	>4.42
Kepler-423	$2.68 \pm 7 \times 10^{-8}$	22 ± 0.121	0.85 ± 0.04	0.95 ± 0.04	0.59 ± 0.081	1.19 ± 0.052	$5.3^{+0.189}_{-0.21}$
Kepler-44	$3.25 \pm 3 \times 10^{-6}$	17 ± 8.6	1.12 ± 0.08	1.35 ± 0.08	1 ± 0.1	1.09 ± 0.07	>4.46
Kepler-45	$2.46 \pm 4 \times 10^{-6}$	15.8 ± 0.002	0.59 ± 0.06	0.55 ± 0.11	0.51 ± 0.09	0.96 ± 0.11	>4.19
Qatar-1	$1.42 \pm 2.2 \times 10^{-7}$	23.7 ± 0.5	0.84 ± 0.04	0.8 ± 0.02	$1.29^{+0.052}_{-0.049}$	$1.14^{+0.026}_{-0.025}$	$7.21^{+0.639}_{-0.293}$
Qatar-2	$1.34 \pm 2.6 \times 10^{-7}$	11.4 ± 0.5	0.74 ± 0.02	0.78 ± 0.01	2.49 ± 0.054	1.25 ± 0.013	$6.78^{+0.0725}_{-0.0729}$
TrES-2	$2.47 \pm 9 \times 10^{-8}$	25 ± 19	0.98 ± 0.06	$1^{+0.04}_{-0.03}$	1.2 ± 0.068	1.22 ± 0.041	>5.10
TrES-3	1.30618581	28 ± 19	0.93 ± 0.05	0.83 ± 0.02	$1.91^{+0.075}_{-0.08}$	$1.34^{+0.031}_{-0.037}$	>6.61
TrES-5	$1.48 \pm 6.14 \times 10^{-6}$	11.6 ± 1.11	0.9 ± 0.03	0.87 ± 0.01	1.79 ± 0.068	1.21 ± 0.021	$6.37^{+0.263}_{-0.251}$
WASP-104	$1.76^{+1.8 \times 10^{-6}}_{-3.6 \times 10^{-6}}$	$1 \times 10^2 \pm 2 \times 10^2$	1.08 ± 0.05	0.96 ± 0.03	1.27 ± 0.047	1.14 ± 0.037	>6.76
WASP-114	$1.55^{+1.2 \times 10^{-6}}_{-9.1 \times 10^{-7}}$	11 ± 1.3	1.29 ± 0.05	1.43 ± 0.06	1.77 ± 0.064	1.34 ± 0.064	$6.41^{+0.319}_{-0.293}$
WASP-119	$2.5 \pm 1 \times 10^{-5}$	$9 \times 10^1 \pm 1 \times 10^2$	1.02 ± 0.06	1.2 ± 0.1	1.23 ± 0.08	1.4 ± 0.2	>6.22
WASP-123	$2.98 \pm 2.3 \times 10^{-6}$	65 ± 45	1.17 ± 0.06	1.28 ± 0.05	0.899 ± 0.036	1.33 ± 0.074	>5.92
WASP-124	$3.37 \pm 1 \times 10^{-6}$	16 ± 4.5	1.07 ± 0.05	1.02 ± 0.02	0.6 ± 0.07	1.24 ± 0.03	>4.16
WASP-133	$2.18 \pm 1 \times 10^{-6}$	$2 \times 10^2 \pm 6 \times 10^2$	1.16 ± 0.08	1.44 ± 0.05	1.16 ± 0.09	1.21 ± 0.05	>7.02
WASP-135	$1.4 \pm 8 \times 10^{-7}$	10 ± 2.1	0.98 ± 0.06	0.96 ± 0.05	1.9 ± 0.08	1.3 ± 0.09	$6.57^{+0.541}_{-0.557}$
WASP-140	$2.24 \pm 8 \times 10^{-7}$	10.4 ± 0.5	0.9 ± 0.04	0.87 ± 0.04	2.44 ± 0.07	$1.4^{+0.42}_{-0.18}$	$5.82^{+0.181}_{-0.149}$
WASP-141	$3.31 \pm 5 \times 10^{-6}$	18 ± 3.8	1.25 ± 0.06	1.37 ± 0.07	2.69 ± 0.15	1.21 ± 0.08	>5.86
WASP-19	$0.789 \pm 4 \times 10^{-8}$	11.8 ± 0.5	0.9 ± 0.04	1 ± 0.02	$1.07^{+0.038}_{-0.037}$	1.39 ± 0.032	$6.86^{+0.0491}_{-0.0472}$
WASP-23	$2.94^{+1.1 \times 10^{-6}}_{-1.3 \times 10^{-6}}$	18 ± 2.7	0.78 ± 0.13	0.77 ± 0.05	$0.884^{+0.088}_{-0.099}$	$0.962^{+0.047}_{-0.056}$	$6^{+1.6}_{-1.4}$
WASP-26	$2.76 \pm 6.7 \times 10^{-6}$	17 ± 1.9	1.11 ± 0.03	1.3 ± 0.06	1.03 ± 0.021	1.28 ± 0.075	$5.64^{+0.34}_{-0.298}$
WASP-36	$1.54 \pm 2.4 \times 10^{-7}$	15 ± 5.5	1.08 ± 0.03	0.98 ± 0.01	2.36 ± 0.07	1.27 ± 0.03	>5.99
WASP-4	$1.34 \pm 3.1 \times 10^{-7}$	22.2 ± 0.5	0.89 ± 0.01	0.92 ± 0.06	1.22 ± 0.013	1.21 ± 0.07	$7.09^{+0.262}_{-0.204}$
WASP-41	$3.05 \pm 9 \times 10^{-7}$	18.4 ± 0.5	0.93 ± 0.07	0.87 ± 0.03	0.94 ± 0.05	1.21 ± 0.07	$5.31^{+1.27}_{-0.387}$
WASP-43	$0.813 \pm 1 \times 10^{-6}$	15.6 ± 0.5	0.58 ± 0.05	0.6 ± 0.04	1.78 ± 0.1	$0.93^{+0.07}_{-0.09}$	$7.6^{+0.185}_{-0.189}$
WASP-44	$2.42 \pm 8.7 \times 10^{-6}$	15 ± 4.3	0.95 ± 0.03	0.93 ± 0.07	0.889 ± 0.062	$1.1^{+0.13}_{-0.14}$	>4.26
WASP-46	$1.43 \pm 9.3 \times 10^{-7}$	16.1 ± 1	0.83 ± 0.08	0.86 ± 0.03	1.91 ± 0.13	1.33 ± 0.058	$7^{+0.252}_{-0.247}$
WASP-49	$2.78 \pm 5.6 \times 10^{-6}$	55 ± 18	0.94 ± 0.08	0.98 ± 0.03	0.378 ± 0.027	1.11 ± 0.047	>5.69
WASP-5	$1.63^{+2.2 \times 10^{-6}}_{-4.9 \times 10^{-6}}$	17 ± 2.5	$0.96^{+0.13}_{-0.09}$	$1.03^{+0.06}_{-0.07}$	$1.58^{+0.13}_{-0.1}$	1.15 ± 0.048	$6.22^{+0.33}_{-0.329}$
WASP-50	$1.96 \pm 5.1 \times 10^{-6}$	16.3 ± 0.5	0.89 ± 0.08	0.84 ± 0.03	$1.47^{+0.091}_{-0.086}$	1.15 ± 0.048	$6.08^{+0.113}_{-0.12}$
WASP-52	$1.75 \pm 1.2 \times 10^{-6}$	16.4 ± 0.5	0.87 ± 0.03	0.79 ± 0.02	0.46 ± 0.02	1.27 ± 0.03	>4.54
WASP-57	$2.84 \pm 8.1 \times 10^{-7}$	13 ± 4.5	0.89 ± 0.07	0.93 ± 0.03	0.644 ± 0.062	$0.916^{+0.017}_{-0.014}$	>3.30
WASP-6	$3.36 \pm 3.1 \times 10^{-7}$	23.8 ± 0.5	0.84 ± 0.06	0.86 ± 0.02	0.485 ± 0.027	0.86 ± 0.12	>4.93
WASP-64	$1.57 \pm 1.5 \times 10^{-6}$	16 ± 3.7	1 ± 0.03	1.06 ± 0.03	1.27 ± 0.068	1.27 ± 0.039	$6.37^{+0.536}_{-0.564}$

Table 1 continued

Table 1 *(continued)*

System	Orbital Period	Spin Period	Stellar Mass	Stellar Radius	Planetary Mass	Planetary Radius	$\log_{10}(Q'_\star)$
	[days]	[days]	[$M_\odot$]	[$R_\odot$]	[M_J]	[R_J]	
WASP-65	$2.31\pm1.5\times10^{-6}$	14 ± 2.1	0.93 ± 0.14	1.01 ± 0.05	1.6 ± 0.16	1.11 ± 0.059	$5.91^{+0.244}_{-0.252}$
WASP-77 A	$1.36\pm2\times10^{-6}$	15.4 ± 0.5	1 ± 0.04	0.95 ± 0.01	1.76 ± 0.06	1.21 ± 0.02	$6.87^{+0.0745}_{-0.0763}$
WASP-80	$3.07^{+8.3\times10^{-7}}_{-7.9\times10^{-7}}$	24 ± 3	0.58 ± 0.05	0.59 ± 0.02	$0.538^{+0.035}_{-0.036}$	$0.952^{+0.026}_{-0.027}$	$5.4^{+3.1}_{-1.3}$
WASP-81	$2.72\pm2.3\times10^{-6}$	54 ± 33	1.08 ± 0.06	1.28 ± 0.04	$0.729^{+0.036}_{-0.035}$	$1.43^{+0.051}_{-0.046}$	>5.72
WASP-95	$2.18\pm1.4\times10^{-6}$	20.7 ± 2	1.11 ± 0.09	$1.13^{+0.08}_{-0.04}$	$1.13^{+0.1}_{-0.04}$	1.21 ± 0.06	>5.74
WASP-96	$3.43\pm2.7\times10^{-6}$	35 ± 31	1.06 ± 0.09	1.05 ± 0.05	0.48 ± 0.03	1.2 ± 0.06	>4.28
WASP-97	$2.07\pm1\times10^{-6}$	49 ± 22	1.12 ± 0.06	1.06 ± 0.04	1.32 ± 0.05	1.13 ± 0.06	>6.49
WASP-98	$2.96\pm4.3\times10^{-7}$	$4\times10^1\pm4\times10^1$	0.81 ± 0.06	0.74 ± 0.02	0.922 ± 0.08	1.1 ± 0.04	$6.5^{+1.8}_{-1.5}$
WTS-2	$1.02\pm6.5\times10^{-7}$	17 ± 7.9	0.82 ± 0.08	0.75 ± 0.03	1.1 ± 0.16	1.36 ± 0.061	>5.84
XO-2 N	$2.62\pm2.8\times10^{-7}$	48 ± 5.7	0.97 ± 0.05	$1.01^{+0.1}_{-0.07}$	0.597 ± 0.021	1.02 ± 0.031	>6.11

REFERENCES

Albrecht, S., Winn, J. N., Johnson, J. A., et al. 2012, ApJ, 757, 18

Bonomo, A. S., Desidera, S., Benatti, S., et al. 2017, ArXiv e-prints, arXiv:1704.00373

Choi, J., Dotter, A., Conroy, C., et al. 2016, ApJ, 823, 102

Christensen-Dalsgaard, J., Däppen, W., Ajukov, S. V., et al. 1996, Science, 272, 1286

Crida, A., & Batygin, K. 2014, A&A, 567, A42

Dawson, R. I., Murray-Clay, R. A., & Johnson, J. A. 2015, ApJ, 798, 66

Debes, J. H., & Jackson, B. 2010, ApJ, 723, 1703

Dotter, A. 2016, The Astrophysical Journal Supplement Series, 222, 8

Essick, R., & Weinberg, N. N. 2016, ApJ, 816, 18

Fabrycky, D., & Tremaine, S. 2007, ApJ, 669, 1298

Gallet, F., & Bouvier, J. 2015, A&A, 577, A98

Goldreich, P. 1963, MNRAS, 126, 257

Goldreich, P., & Keeley, D. A. 1977, ApJ, 211, 934

Goldreich, P., & Kumar, P. 1988, ApJ, 326, 462

Goldreich, P., Murray, N., & Kumar, P. 1994, ApJ, 424, 466

Goldreich, P., & Soter, S. 1966, Icarus, 5, 375

Gonczi, G. 1981, A&A, 96, 138

Goodman, J., & Dickson, E. S. 1998, ApJ, 507, 938

Hansen, B. M. S. 2010, ApJ, 723, 285

Hebb, L., Collier-Cameron, A., Triaud, A. H. M. J., et al. 2010, ApJ, 708, 224

Hébrard, G., Bouchy, F., Pont, F., et al. 2008, A&A, 488, 763

Husnoo, N., Pont, F., Mazeh, T., et al. 2012, MNRAS, 422, 3151

Irwin, J., Hodgkin, S., Aigrain, S., et al. 2007, MNRAS, 377, 741

Jackson, B., Greenberg, R., & Barnes, R. 2008, ApJ, 678, 1396

Lai, D. 2012, MNRAS, 423, 486

Li, G., & Winn, J. N. 2016, ApJ, 818, 5

Lin, D. N. C., Bodenheimer, P., & Richardson, D. C. 1996, Nature, 380, 606

Maciejewski, G., Dimitrov, D., Fernández, M., et al. 2016, A&A, 588, L6

Mazeh, T. 2008, in EAS Publications Series, Vol. 29, EAS Publications Series, ed. M.-J. Goupil & J.-P. Zahn, 1–65

Meibom, S., & Mathieu, R. D. 2005, ApJ, 620, 970

Milliman, K. E., Mathieu, R. D., Geller, A. M., et al. 2014, AJ, 148, 38

Naoz, S., Farr, W. M., & Rasio, F. A. 2012, ApJL, 754, L36

Narita, N., Sato, B., Hirano, T., & Tamura, M. 2009, PASJ, 61, L35

Nelson, B. E., Ford, E. B., & Rasio, F. A. 2017, AJ, 154, 106

Ngo, H., Knutson, H. A., Hinkley, S., et al. 2015, ApJ, 800, 138

—. 2016, ApJ, 827, 8

Ogilvie, G. I. 2014, ARA&A, 52, 171

Ogilvie, G. I., & Lin, D. N. C. 2004, ApJ, 610, 477

Patra, K. C., Winn, J. N., Holman, M. J., et al. 2017, ArXiv e-prints, arXiv:1703.06582

Paxton, B., Bildsten, L., Dotter, A., et al. 2011, ApJS, 192, 3

Paxton, B., Cantiello, M., Arras, P., et al. 2013, ApJS, 208, 4

Paxton, B., Marchant, P., Schwab, J., et al. 2015, ApJS, 220, 15

Penev, K., Barranco, J., & Sasselov, D. 2009, ApJ, 705, 285

Penev, K., Jackson, B., Spada, F., & Thom, N. 2012, ApJ, 751, 96

Penev, K., Zhang, M., & Jackson, B. 2014, PASP, 126, 553

Penev, K., Hartman, J. D., Bakos, G. Á., et al. 2016, AJ, 152, 127

Petrovich, C. 2015, ApJ, 799, 27

Pont, F. 2009, MNRAS, 396, 1789

Queloz, D., Anderson, D. R., Collier Cameron, A., et al. 2010, A&A, 517, L1

Rasio, F. A., & Ford, E. B. 1996, Science, 274, 954

Rogers, T. M., & Lin, D. N. C. 2013, ApJL, 769, L10

Schatzman, E. 1962, Annales d'Astrophysique, 25, 18. http://adsabs.harvard.edu/abs/1962AnAp...25...18S

Schlaufman, K. C., & Winn, J. N. 2013, ApJ, 772, 143

—. 2016, ApJ, 825, 62

Skumanich, A. 1972, The Astrophysical Journal, 171, 565. http://adsabs.harvard.edu/abs/1972ApJ...171..565S

Valsecchi, F., & Rasio, F. A. 2014, ApJ, 786, 102

van Saders, J. L., Ceillier, T., Metcalfe, T. S., et al. 2016, Nature, 529, 181

Weber, E. J., & Davis, Jr., L. 1967, The Astrophysical Journal, 148, 217. http://adsabs.harvard.edu/abs/1967ApJ...148..217W

Winn, J. N., Fabrycky, D., Albrecht, S., & Johnson, J. A. 2010, ApJL, 718, L145

Winn, J. N., Johnson, J. A., Albrecht, S., et al. 2009, ApJL, 703, L99

Winn, J. N., Johnson, J. A., Marcy, G. W., et al. 2006, ApJL, 653, L69

Zahn, J.-P. 1975, A&A, 41, 329

—. 1989, A&A, 220, 112